Nanoscale

PAPER

View Article Online
View Journal | View Issue

Cite this: *Nanoscale*, 2015, **7**, 16470

Magnetic nanoparticle-conjugated polymeric micelles for combined hyperthermia and chemotherapy†

Hyun-Chul Kim,*[a] Eunjoo Kim,*[a] Sang Won Jeong,[a] Tae-Lin Ha,[a] Sang-Im Park,[a] Se Guen Lee,[a] Sung Jun Lee[a] and Seung Woo Lee[b]

Received 22nd June 2015,
Accepted 6th August 2015

DOI: 10.1039/c5nr04130a

www.rsc.org/nanoscale

Magnetic nanoparticle-conjugated polymeric micelles (MNP-PMs) consisting of poly(ethylene glycol)-poly(lactide) (PEG-PLA) and iron oxide nanoparticles were prepared and used as nanocarriers for combined hyperthermia and chemotherapy. Doxorubicin (DOX) was encapsulated in MNP-PMs, and an alternating magnetic field (AMF) resulted in an increase to temperature within a suitable range for inducing hyperthermia and a higher rate of drug release than observed without AMF. *In vitro* cytotoxicity and hyperthermia experiments were carried out using human lung adenocarcinoma A549 cells. When MNP-PMs encapsulated with an anticancer drug were used to treat A549 cells in combination with hyperthermia under AMF, 78% of the cells were killed by the double effects of heat and the drug, and the combination was more effective than either chemotherapy or hyperthermia treatment alone. Therefore, MNP-PMs encapsulated with an anticancer drug show potential for combined chemotherapy and hyperthermia.

1. Introduction

Magnetic nanoparticles (MNPs) have emerged as a key material for many biomedical applications, such as drug delivery systems, magnetic resonance imaging and magnetic hyperthermia.[1–4] Magnetic hyperthermia is a particularly attractive medical therapeutic approach, which is based on the induction heating of MNPs under application of an alternating magnetic field (AMF).[5–7] In the past decade, this technique has been developed as a therapeutic modality to treat cancer by maintaining the temperature of the tumor region at 41–46 °C to inhibit the regulatory and growth processes of cancerous cells.[5–7] MNPs are often incorporated or conjugated in polymer systems, such as hydrogels,[8] spheres, liposomes,[9,10] and micelles,[11–13] to magnetically guide the nanoparticles to the tumor site,[14,15] or to release a drug in a controlled manner upon deformation in a magnetic field or due to hyperthermia under AMF.[16] Thermosensitive polymers are typically used for hyperthermia induction and the resulting temperature change alters their volume and causes a shape collapse. Using a composite of MNPs and thermosensitive polymers, loaded with an anticancer drug, exposure to an AMF has been shown to lead to an increase in cell death.[17–21] In addition, other research groups have demonstrated that capsules prepared by a combination of mesoporous silica nanoparticles and a polymer could accommodate both anticancer drugs and MNPs to exert an increased cell toxicity effect through rapid release of the drug and hyperthermia under AMF.[22–24] In all cases, the enhanced therapeutic effect observed was ascribed to the combination of a hyperthermic effect and enhanced drug release. Therefore, the main objective of this study was to develop MNP-based polymeric micelles (PMs) and examine their clinical potential for combined cancer hyperthermia and drug delivery. We here report MNP-PMs with both heat-generating and drug-releasing abilities for enhanced hyperthermic chemotherapy. PMs and MNPs serve as cargo of the drug and heat source, respectively. Here, we employed poly(ethylene glycol)-poly(lactide) (PEG-PLA) as the polymer, because Yamamoto *et al.*[25] suggested that the critical change in PEG-PLA micelles occurring around the physiological temperature range shows their possibility for use in drug therapy combined with local heat treatment. As drug carriers, the outer hydrophilic PEG chain plays the role of a palisade to avoid protein adsorption and subsequent non-specific uptake by the mononuclear phagocytic system.[26–28] On the other hand, the inner core composed of PLA chains regulates the retention and release of

[a]*Division of Nano and Energy Convergence Research, Daegu Gyeongbuk Institute of Science and Technology (DGIST), Daegu 711-873, Korea. E-mail: kimhc@dgist.ac.kr, ejkim@dgist.ac.kr; Fax: +82-53-785-3559, +82-53-785-3559; Tel: +82-53-785-2540, +82-53-785-2530*
[b]*School of Chemical Engineering, Yeungnam University, Gyeongbuk 712-749, Korea*
†Electronic supplementary information (ESI) available. See DOI: 10.1039/c5nr04130a

drug molecules on an appropriate time scale.[29] PEG-PLA-NH_2, containing an amino group, was synthesized by modification of the hydroxyl group of the PLA end. The surface of Fe_3O_4 nanoparticles was coated with citric acid (CA), and MNP-conjugated PLA-PEG was prepared by an amidation reaction of PEG-PLA-NH_2 and the CA-coated Fe_3O_4 nanoparticles. Doxorubicin (DOX) was encapsulated in the MNP-PMs for combined cancer hyperthermia and drug delivery. The heating pattern and DOX release from the DOX/MNP-PMs was evaluated by applying AMF. Furthermore, an *in vitro* hyperthermia experiment under AMF for DOX/MNP-PMs was performed in a cellular environment using confocal laser-scanning microscopy to monitor cellular uptake, and cell viability assays were conducted to evaluate their thermo-and chemo-therapeutic effects.

2 Experimental

2.1 Materials

Methoxypoly(ethylene glycol)-*co*-poly(D,L-lactide) (mPEG-PLA) comprising PEG with a molecular weight of 5000 g mol^{-1} and PDLLA with a molecular weight of 3000 g mol^{-1} was purchased from Polysciences. 6-(Butoxycarbonyl-amino)caproic acid (Boc-6-Ahx-OH, 99%), *N*,*N*′-dicyclohexylcarboiimide (DCC, 99%), *N*-(3-dimethylaminopropyl)-*N*′-ethylcarbodiimide hydrochloride (EDC, 98%), trifluoroacetic acid (TFA, 99%), *N*-hydroxysuccinimide (NHS, 98%), $FeCl_3{\cdot}6H_2O$ (98%), sodium oleate (95%), oleylamine (70%), oleic acid (90%), and citric acid (CA, 99%) were purchased from Sigma-Aldrich and used as received. All solvents were obtained from commercial suppliers and were used without further purification.

2.2 Measurements

Nuclear magnetic resonance (NMR) spectra were obtained using a Bruker NMR spectrometer (AVANCE III 400). Fourier transform-infrared (FT-IR) spectra were obtained with a Thermo-Nicolet IR spectrometer (IR380) on solid samples. Thermogravimetric analysis (TGA) was performed at a temperature range of 30–700 °C with a heating rate of 10 °C min^{-1} under nitrogen, using the TGA-600 system (TA Instruments). The intrinsic magnetic properties were measured by generating a magnetic hysteresis loop using a vibrating sample magnetometer (VSM; Lakeshore 7300) in the magnetic field strength range of ±10 kOe. The size and size distribution of the hydrodynamic diameter by volume were measured using dynamic light scattering (DLS; Zetasizer Nano ZS, Malvern Instruments). Nanostructures of magnetic nanoparticles were examined using transmission electron microscopy (TEM; HF-3300, Hitachi). The samples were stained with uranyl acetate. UV-vis absorption spectra were obtained using a Cary 100 Conc UV-vis spectrometer (Varian).

2.3 Synthesis

2.3.1. Synthesis of Boc-Ahx-PLA-PEG. mPEG-PLA (2.0 g, 0.25 mmol) was dissolved in anhydrous dichloromethane (50 mL). Boc-6-Ahx-OH (0.12 g, 0.5 mmol) was added to this solution, followed by DCC (0.1 g, 0.5 mmol). The reaction mixture was stirred for 48 h at room temperature. When the reaction was complete, the dicyclohexylurea was removed by filtration. Excess acetone was added to the crude product to precipitate the residual dicyclohexylurea. After the precipitates were filtered out, the solvent was removed by rotary evaporation. The product was precipitated from an excess of cold diethyl ether. The polymer was collected and dried under vacuum to give Boc-Ahx-PLA-PEG with a yield of 1.9 g. ^{1}H NMR δ (ppm): 5.18 (m, –C(O)*CH*(CH_3)O–), 3.63 (m, $CH_3OCH_2CH_2O$–), 3.40 (s, $CH_3OCH_2CH_2O$–), 1.70 (d, –C(O)$CH_2(CH_2)_2CH_2NH$–), 1.56 (m, –C(O)CH(CH_3)O–), 1.49 (d, –C(O)OC(CH_3)$_3$).

2.3.2. Synthesis of NH_2-PLA-PEG. Boc-Ahx-PLA-PEG (1.5 g) was dissolved in a mixture of dichloromethane (10 mL) and TFA (5 mL). The solution was stirred at room temperature for 2 h. The solution was concentrated and the crude product was precipitated from cold diethyl ether. The polymer was collected and dried under vacuum at room temperature with a yield of 1.2 g. ^{1}H NMR δ (ppm): 5.18 (m, –C(O)*CH*(CH_3)O–), 3.63 (m, $CH_3OCH_2CH_2O$–), 3.40 (s, $CH_3OCH_2CH_2O$–), 1.70 (d, –C(O)$CH_2(CH_2)_2CH_2NH$–), 1.56 (m, –C(O)CH(CH_3)O–).

2.3.3. Synthesis of CA-coated MNPs (CA-MNPs). Fe_3O_4 nanoparticles and CA-MNPs were prepared as previously reported.[30,31] Briefly, iron chloride hexahydrate (5.4 g, 20 mmol) and sodium oleate (18.3 g, 60 mmol) were dissolved in a mixture composed of 30 mL distilled water, 40 mL ethanol, and 70 mL hexane. The resulting solution was heated to 70 °C and maintained at that temperature for 4 h. After the reaction, the organic layer containing the iron–oleate complex was washed with distilled water three times. Hexane was evaporated off, resulting in the iron–oleate complex. The iron–oleate complex (18 g, 20 mmol), oleylamine (1.0 g, 3.75 mmol), and oleic acid (0.5 g, 1.8 mmol) were dissolved in 100 g of 1-octadecene. The mixture was heated to 320 °C with a constant heating rate of 3 °C min^{-1}, and then kept at that temperature for 30 min. When the initial transparent solution became turbid and brownish black, the resulting solution was cooled to room temperature. The solvent mixture composed of hexane and acetone (250 mL, 1 : 3 v/v ratio) was added to the solution to precipitate the nanoparticles, which were separated by centrifugation. The oleic acid- and oleyl amine-coated nanoparticles (120 mg) prepared as described above were dispersed in a 0.75/0.25 mixture of 1,2-dichlorobenzene and *N*,*N*′-dimethylformamide (15 mL of total volume), to which CA (0.24 g, 1.25 mmol) was added. The mixture was stirred at 100 °C for 24 h. The particles were precipitated by the addition of ethyl ether and recovered by means of an electromagnet. To remove the free CA, the particles were redispersed in distilled water and recovered by means of an electromagnet. This process was repeated three times. The particles were then dried in a vacuum oven for 24 h at 100 °C.

2.3.4. Preparation of PLA-PEG-coated MNPs. CA-MNPs (50 mg) were dispersed in 10 mL of dimethyl sulfoxide (DMSO). To this solution, 0.05 g of EDC and 0.07 g of NHS were added, followed by 0.1 g of NH_2-PLA-PEG. The mixture

was stirred at room temperature for 48 h. Excess ethyl ether was added to the solution to precipitate, and then the precipitate was filtered. For the removal of free CA-MNPs, the resulting product was dissolved in chloroform and then the organic layer was washed three times with distilled water in a separatory funnel. After washing, the chloroform was evaporated off, resulting in solid-form MNPs-PLA-PEG. The MNPs-PLA-PEG were dispersed in distilled water and dialyzed for 3 days using a cellulose membrane with pores at a cut-off size of 12 kDa to remove the unreacted NH_2-PLA-PEG.

2.4 Magnetization setup

A homemade heat induction system was constructed to monitor the temperature change ($\Delta T/\Delta t$) of the MNPs during excitation (Fig. S1 in the ESI†). The system was composed of a power generator (AG1006; 200 W with RF power from 20 kHz to 14 MHz), a high frequency magnetic field generator (MS300k-6A), a thermosensor (Luxtron Fluoroptic Thermometer Model 502), a circulation cooling system, a magnetic core with 20 turns of a 3-Φ copper coil, and the data recording devices. The specimen area was surrounded by a polycarbonate frame (body and cap) to prevent any possible direct heat exchange through the inductive coils. The core structure can reduce the demagnetization factor by tailoring the electric current flow on the surface of the core. A capacitor was added to the circuit to maximize the amplifier's capability by tuning the resonance with the coil's impedance (~4 Ω at 200 kHz). The sample solutions were placed at the center of the coil. The height of the samples was shorter than that of the magnetic induction coil to allow for uniform magnetic field exposure. The field strength was determined from the peak-to-peak difference of the generated sinusoidal wave function. The temperature rise was measured using a fluoro-optic thermometer fiber probe in real-time.

2.5 Drug loading and DOX release from MNP-PMs encapsulated with DOX

For loading of DOX in the MNP-PLA-PEG micelles, DOX (4 mg) was dissolved in dimethylformamide (DMF, 1 mL) along with MNPs-PLA-PEG (20 mg). Phosphate-buffered saline (PBS, 20 mL) was added to the solution while stirring at room temperature. After stirring for 6 h, the resulting mixtures were dialyzed (MWCO: ~2 kDa) against distilled water for 3 days to remove any unloaded DOX and DMF. The external water was changed twice a day. After dialysis, the solutions were passed through a syringe filter (0.45 μm pore size) to remove large aggregates. MNP-PMs encapsulated with DOX (DOX/MNP-PMs) were freeze-dried and re-dissolved in DMF (4 mL), followed by UV/vis spectral analysis. A calibration curve was obtained over various concentrations of DOX in DMF (Fig. S2 in the ESI†), and the DOX loading content was calculated by the ratio of the weight of loaded DOX to that of the dried sample. DOX release from DOX/MNP-PMs was investigated at 37 °C and 45 °C in PBS. AMF was applied at 1.5 kA m^{-1} and 200 kHz. Variations of temperature inside the sample were monitored using a fluoro-optic thermometer fiber probe. The amount of DOX released was measured by using a UV/vis spectrometer.

2.6 Cell culture

Human lung adenocarcinoma A549 (ATCC® CCL-185™) cells were grown in F-12K medium (HyClone) supplemented with 10% fetal bovine serum. Cells were maintained at 37 °C, and 5% CO_2 in a humidified incubator with the medium changed every other day.

2.7 Cytotoxicity and cellular uptake of MNP-PMs

The cytotoxicity of the MNP-PMs was determined by a 3-(4,5-dimethylthiazol-2-yl)-5-(3-carboxymethoxyphenyl)-2-(4-sulfophenyl)-2*H*-tetrazolium) (MTS) assay using a CellTiter 96 kit (Promega) on A549 cells. Cells were seeded at a density of 5 × 104 cells per mL in a 96-well plate with 100 μL of medium, and were incubated for 24 h to allow them to adhere to the surface of the plate. Aliquots of PBS buffer solution containing various concentrations of MNP-PMs were added to each well, and the cells were incubated for a further 48 h. Culture media containing MNP-PMs were removed from the culture plate prior to the addition of 20 μL of the MTS reagent in order to refresh the culture media to prevent any interference in the absorbance measurements. After incubation at 37 °C for 3 h, the absorbance was detected at 490 nm with a microplate reader (Multiskan, Thermo Scientific). The cytotoxicity is expressed as the percentage cell viability with respect to the control cells. To analyze the uptake and distribution of MNP-PMs in cells, a hydrophobic fluorescence dye (Chromis 500N-Azide, λ_{em}506 nm, Cyanogen, Italy) was encapsulated in the MNP-PMs. A549 cells were seeded in a 35 mm cover-glass bottom dish (SPL Life Science, Pocheon-Si, Korea) at a density of 5×10^4 cells per mL and cultured for 24 h. The medium was replaced, and fluorescence dye-encapsulated MNP-PMs were added to the cells at a concentration of 25 μg mL^{-1} for 2 h. The cells were observed under a confocal laser-scanning microscope (LSM 7, Carl Zeiss, Wetzlar, Germany) at excitation with 488 nm, and the emission light was passed through the LP 490 filter.

2.8 Cytotoxicity of MNP-PMs encapsulated with DOX

To observe the cytotoxicity of the DOX/MNP-PMs, A549 cells were seeded at a density of 5×10^4 cells per mL in a 96-well plate with 100 μL of medium, and incubated for 24 h. The cells were treated with various concentrations of free DOX and DOX/MNP-PMs (DOX concentration range, 0.032–20 μg mL^{-1}) and incubated for 48 h. Culture medium containing DOX/MNP-PMs was removed from the culture plate prior to the addition of 20 μL of the MTS reagent to refresh the culture medium. After incubation at 37 °C for 3 h, the absorbance was detected at 490 nm with a microplate reader. Cytotoxicity is expressed as the percentage of viable cells with respect to the control cells.

2.9 Magnetic hyperthermia for A549 cells

A549 cells (2×10^5 cells per mL) were seeded in a 35 mm cell culture dish and cultured for 24 h. After incubation for 2 h with 5 μg mL^{-1} free DOX, 25 μg mL^{-1} MNP-PMs, and 25 μg mL^{-1} DOX/MNP-PMs, the cell medium was removed from the culture dish and washed three times with PBS. Then, the culture dish was refreshed with culture medium and tested in a hyperthermia setup by applying an AMF at a frequency of 200 kHz and a magnetic field amplitude of 1.5 kA m^{-1} for 1 h. To evaluate the effect of hyperthermia treatment among samples, control samples were also prepared. A fluoro-optic thermometer fiber probe (Luxtron) was used to measure the temperature every 1 s after switching on the magnetic field. After heating, the cells were harvested and plated in a 96-well plate in triplicate. After 24 h incubation at 37 °C, cell viability was determined by an MTS assay. In addition, the cells were stained with calcein acetoxymethylester (calcein-AM) and ethidium homodimer-1 at 37 °C for 10 min using a LIVE/DEAD® Viability/Cytotoxicity Kit (Life Technologies). Subsequently, the cells were washed with PBS and inspected under a fluorescence microscope (DMI 3000, Leica). The cells were also observed under a confocal laser-scanning microscope by excitation with 488 nm, under the same laser intensity and gain value between samples. The emission light was passed through an LP 490 filter.

2.10 Statistical analysis

Data from three independent experiments were analyzed using the Student's *t*-test and are reported as mean ± SD. Sigma Plot version 12.3 was used (Systat Software, Inc., Chicago, IL, USA) to determine the *p*-values, and a p-value < 0.05 was considered statistically significant.

3 Results and discussion

3.1 Synthesis and characterization of MNP conjugated PLA-PEG

The preparation of the MNP conjugated PLA-PEG is shown schematically in Scheme 1. Amine functionalized PLA-PEG (NH_2-PLA-PEG) was prepared by modification of the hydroxyl group of the PLA end, and is capable of forming a micellar aggregate in aqueous solution, which can be used to create effective anti-biofouling surfaces by PEG chains and plays a role as drug cargo by the hydrophobic interaction between a drug and PLA chains.[26–29] To achieve a grafting density of NH_2-PLA-PEG for coupling with MNPs, several anchor sites are required. Here, CA was used as the exchange ligand to coordinate the multiple carboxylates on the MNP surface. The CA-MNPs can be dispersed in aqueous media such as water, DMF, and DMSO. The free carboxylic acid groups on the surface of MNPs are available for the amidation reaction with the amino group of NH_2-PLA-PEG. After activation of the carboxylic groups on MNPs with EDC and NHS in DMSO, PLA-PEG was linked to the CA-MNPs *via* the amidation reaction with NH_2-PLA-PEG.

The covalent linkage of amine-functionalized PLA-PEG to CA-MNPs was confirmed by FT-IR spectrometry (Fig. 1). The characteristic peaks of Fe_3O_4 nanoparticles appeared between 600 cm^{-1} and 400 cm^{-1}. These broad low-intensity bands can be associated with the stretching and torsional vibration modes of magnetite.[32] The peaks corresponding to the symmetric vibration of C=O at 1693 cm^{-1} and asymmetric C–O stretching at 1419 cm^{-1} from the carboxylic group of CA were shifted to 1579 cm^{-1} and 1362 cm^{-1}, respectively. Two new characteristic peaks were observed due to the presence of the COO–Fe bond, indicating binding by the interaction between

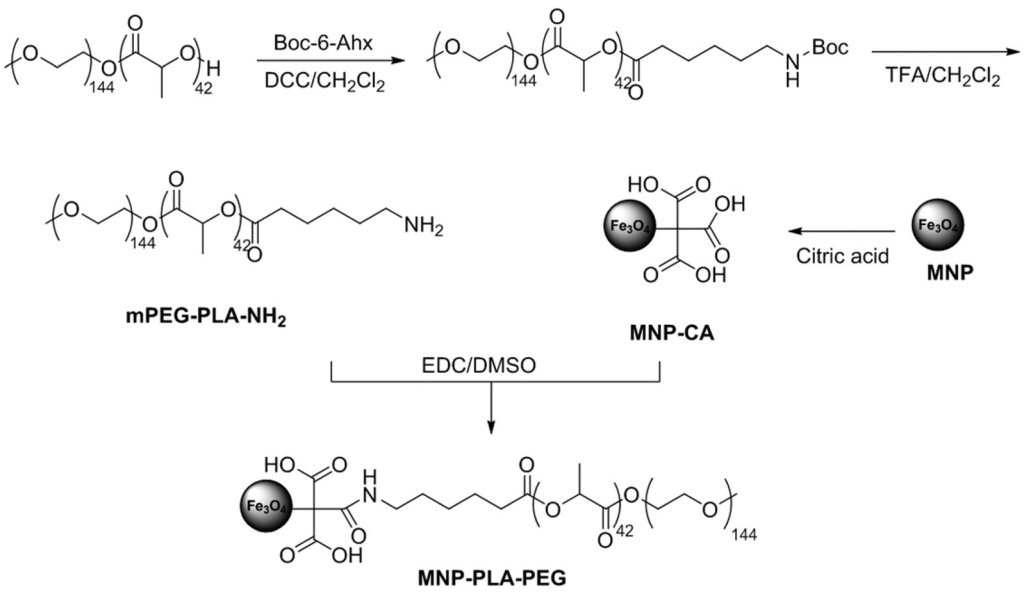

Scheme 1 Synthetic route of magnetic nanoparticle-conjugated poly(ethylene glycol)-poly(lactide) (MNP-PLA-PEG).

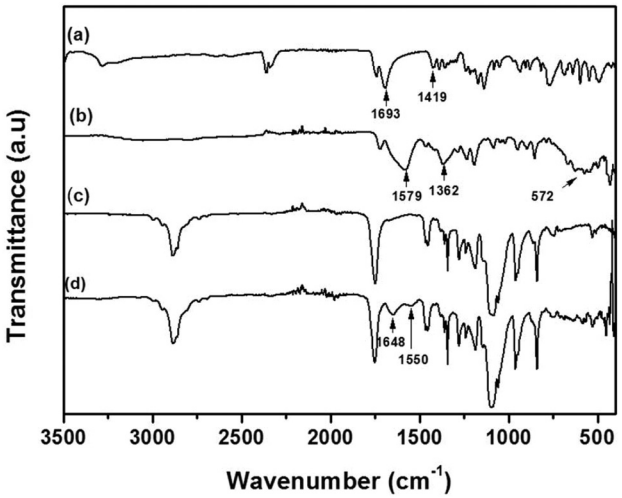

Fig. 1 FT-IR spectra of citric acid (a), citric acid-coated MNPs (b), NH_2-PLA-PEG (c), and MNP-conjugated PLA-PEG (d).

Fe_3O_4 nanoparticles and the carboxylic group of CA. The FT-IR spectrum of MNPs-PLA-PEG exhibited an amide I band due to the C═O stretching vibration at 1648 cm^{-1} and an amide II band caused by the N–H bending motion at 1550 cm^{-1}, which could be assigned to the amide carbonyl groups, indicating the successful linkage of amine-functionalized PLA-PEG to the surface of CA-MNPs *via* the amidation reaction. In addition, peaks at 1751 cm^{-1} and 1096 cm^{-1} appeared in the NH_2-PLA-PEG and MNP-PLA-PEG spectra, which were attributable to the stretching vibration corresponding to the carbonyl of PLA and the ether bonds of PEG chains, respectively.

The amounts of MNPs on the CA and PLA-PEG were assessed by TGA (Fig. S3 in the ESI†). As shown in Table 1, the weight percentages of MNPs on CA and PLA-PEG were 39.5% and 4.0%, respectively. Based on the results of TGA, the amount of CA on the surface of MNPs was calculated to be 3.15 mmol g^{-1} Fe_3O_4. Considering this value, the carboxylic moiety capable of reacting with NH_2-PLA-PEG was predicted to be approximately 9. The increased mass loss for the MNP-PLA-PEG may be due to the introduction of a large amount of PLA-PEG on the surface of MNPs. The saturation magnetization (M_s) curves of CA-MNPs and MNP-PLA-PEG are shown in Fig. S4 of the ESI.† These nanoparticles showed typical superparamagnetic behavior without a hysteresis loop at room temperature. The M_s values for CA-MNPs and MNPs-PLA-PEG were normalized using the weight of iron oxide nanoparticles measured by TGA, and were calculated to be 12.7 and 0.68 emu g^{-1}, respectively.

The size and size distribution of the MNP-PMs were measured using DLS (Fig. 2(a)). The size determined *via* DLS was in the range of 50–190 nm with an average diameter of 79.8 nm, which is suitable for a drug delivery system to escape from the reticuloendothelial (RES) system.[33] The morphological structures of CA-MNPs and MNP-PMs were analyzed by TEM (Fig. 2(b)). The samples were prepared by drop-coating the sample solutions onto a copper grid, followed by lyophilization. The mean diameter of the CA-MNPs determined by TEM was approximately 8 nm and the CA-MNPs were found to be well-dispersed (Fig. 2(b), inset). Since the organic trace left by coating of CA can hardly be detected by TEM, DLS measurement was performed to evaluate the hydrodynamic diameter of the CA-MNPs in water. As shown in Fig. 2(b), the hydrodynamic diameter of the CA-MNPs was in the range of

Table 1 Magnetization values of citric acid-coated-iron oxide nanoparticles (CA-MNPs) and magnetic nanoparticle-conjugated-PLA-PEG (MNP-PLA-PEG) measured on a vibration sample magnetometer based on thermogravimetric data

Material	Iron oxide (wt%)	$M_{S_{sample}}$ (emu g^{-1})	$M_{S_{Fe}}$ (iron oxide 100%)[a] (emu g^{-1})
CA-MNPs	39.5	12.70	32.15
MNPs-PLA-PEG	4.0	0.68	17.0

[a] Theoretical (calculated) saturation magnetization (M_s) for each particle.

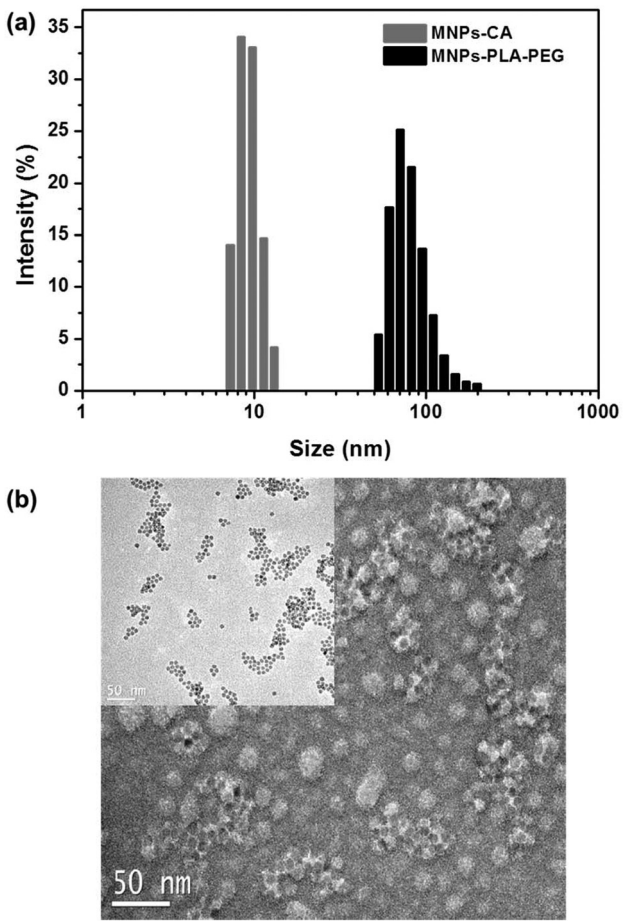

Fig. 2 Size distribution of citric acid-coated MNPs and MNP-PLA-PEG micelles measured by DLS (a), and TEM images of MNP-PLA-PEG micelles (b) (inset of (b): citric acid-coated MNPs; scale bar = 20 nm).

7.5–13.5 nm with an average diameter of 9.6 nm and a polydispersity index (PDI) of 0.30. The size measured from TEM was slightly smaller than that obtained from DLS, which was likely caused by shrinkage of the CA coated on the MNPs during the drying process. The TEM images for the MNP-PMs showed a core–shell structure, wherein the dark interior and the gray exterior correspond to the areas enriched with MNPs and the saturated PLA-PEG, respectively.

3.2 Heating ability under the AC magnetic field

The DOX loading content in the MNP-PMs was determined using DOX as a hydrophobic drug with a DOX : MNP-PLA-PEG feed-weight ratio ($Mass_{DOX}/Mass_{MNPs\text{-}PLA\text{-}PEG}$ = 0.2) of 11.4%. The heating ability of DOX/MNP-PMs with a concentration of 25 μg mL^{-1} was evaluated under the applied field strength (H_0) of 1.5 kA m^{-1} and frequency (f) of 200 kHz; under these conditions, the product cannot exceed 4.85 × 10^8 A m^{-1} s^{-1} to ensure a physiologically tolerable and biologically safe hyperthermia treatment.[34,35] In our experiment, water was supplied *via* a circulation cooling system to maintain a constant temperature of 37 °C. The temperature change of water as the reference was measured under a continuous AC magnetic field. As shown in Fig. 3, the temperature of samples was 30 ± 1 °C at the beginning of the experiment. Therefore, the sample could acquire an additional heat from the cooling system until the temperature of the sample reached 37 °C. The experimental curves of DOX/MNP-PMs under a continuous AC

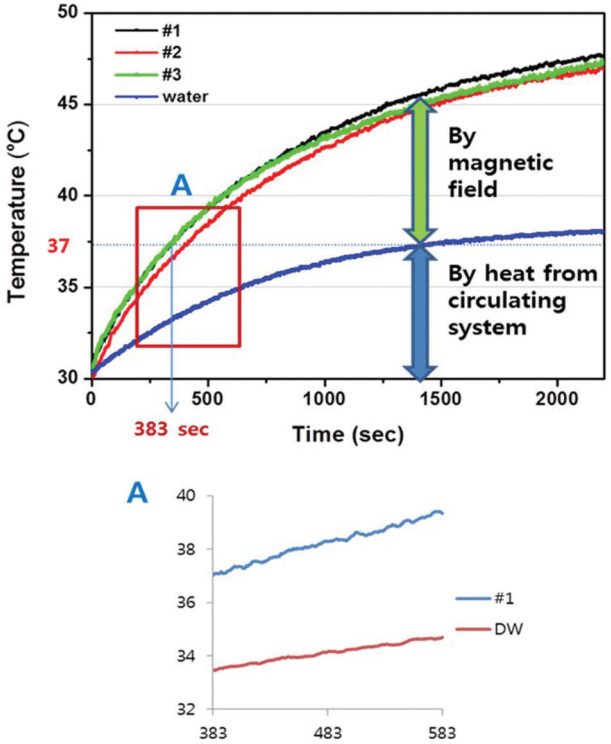

Fig. 3 Temperature profiles of water or DOX/MNP-PLA-PEG micelles under AMF. Panel A shows the linear relationship at 382–583 s, which was the initial time point after sample #1 reached 37 °C.

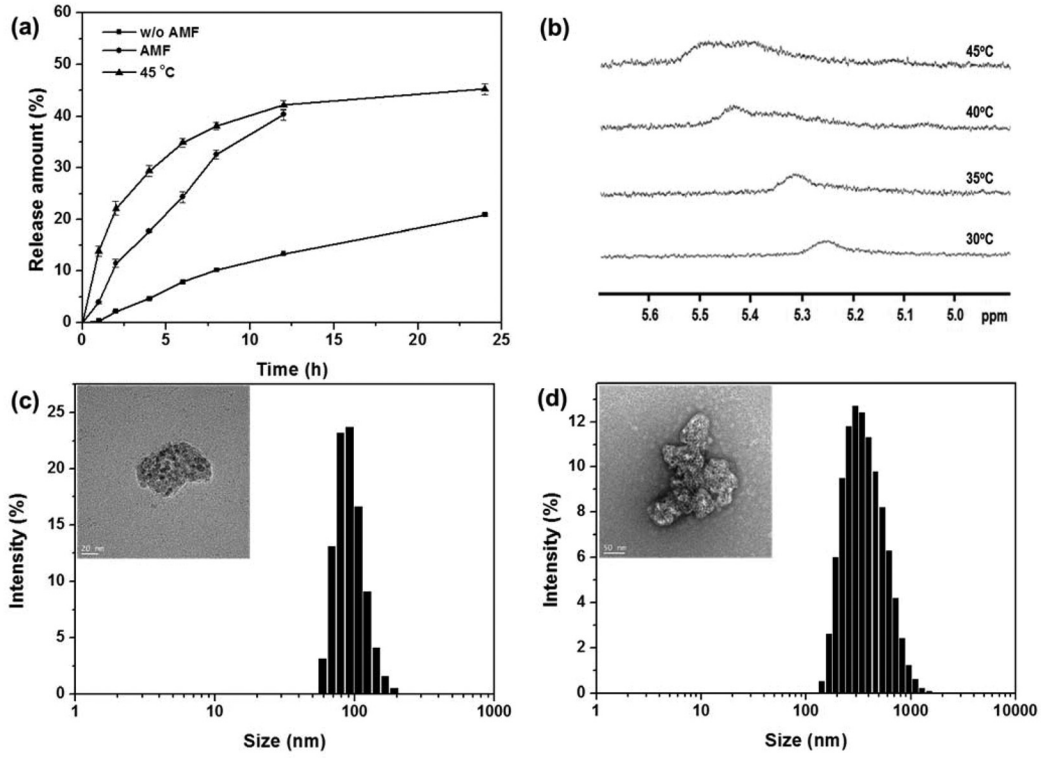

Fig. 4 DOX release from DOX/MNP-PLA-PEG micelles at 25 °C, 45 °C, and under AMF (a); change in the peak profile of the methine proton of MNP-PLA-PEG in ^1H NMR spectra measured at varying temperatures in D_2O (b); size distribution of DOX/ MNP-PLA-PEG micelles before applying AMF (inset: TEM image; scale bar = 20 nm) (c); and size distribution of DOX/MNP-PLA-PEG micelles after applying AMF (inset: TEM image; scale bar = 20 nm) (d).

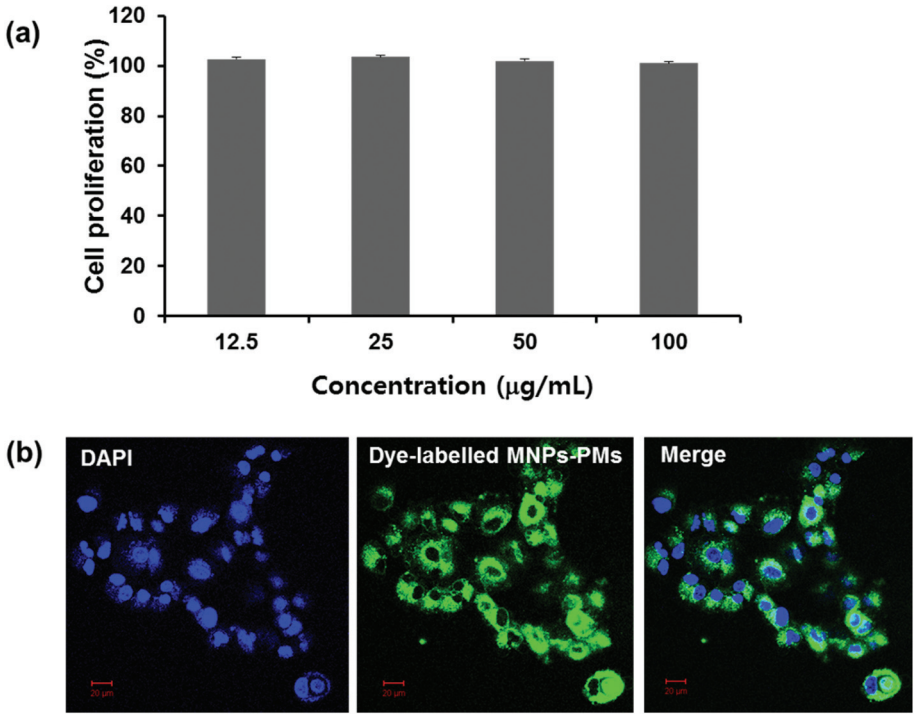

Fig. 5 Viability of A549 cells incubated with varying amounts of MNP-PLA-PEG micelles as determined by an MTS assay (a), and cellular uptake of the fluorescence dye encapsulated MNP-PLA-PEG micelles in A549 cells by confocal laser scanning microscopy (scale bar = 20 μm) (b).

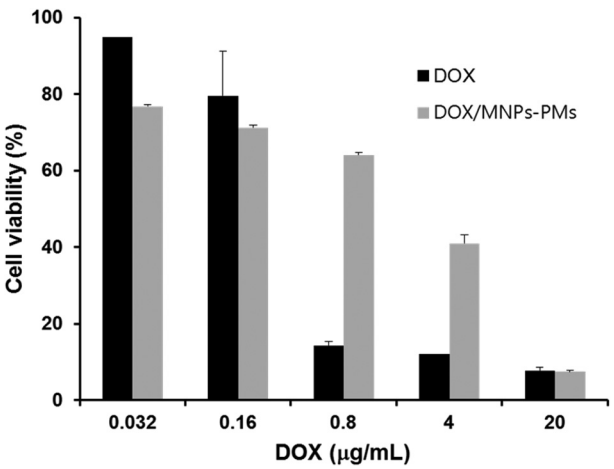

Fig. 6 Viability of A549 cells after incubation for 48 h with different amounts of free DOX or DOX/MNP-PLA-PEG micelles.

magnetic field show the increase of temperature over time. The temperature of the medium gradually increased up to 42 °C after 13 min from the initial set temperature and plateaued at around 45 °C after 25 min. This characteristic may be attributed to heating effects related to the Néel relaxation and Brown rotation of MNPs subjected to an AC magnetic field. Considering that the moderate temperature for hyperthermia is in the range of 41–46 °C, this result is sufficient for hyperthermia applications.

3.3 Drug release mediated by AMF

The DOX release from DOX/MNP-PMs was investigated under an AMF (Fig. 4(a)). DOX release was accelerated further under AMF compared to the tested conditions without the magnetic field. For samples in which AMF was not applied, less than 20% of the encapsulated DOX was released over 24 h, most likely because DOX was confined in the hydrophobic PLA part of the MNP-PMs. As a control, a drug release experiment was performed at 45 °C in the absence of AMF. Drug release at 45 °C was higher with AMF than without, which can be explained by accelerated diffusion of the drug molecules at elevated temperature. Moreover, in order to evaluate whether the enhanced drug release could be due to the mobility change of PLA chains through the local internal heating caused by the MNPs under AMF, ^{1}H NMR measurement of MNP-PMs in D_2O was performed. MNP-PMs were prepared using an organic solvent/water (o/w) emulsion technique in D_2O at a concentration of 10 mg mL^{-1}. The change in the peak shape and position of the methine proton of the PLA segment with increasing temperature are shown in Fig. 4(b) as expanded spectra in the range of 5.0–5.6 ppm. The position of the methine peak was shifted downfield with increasing temperature, demonstrating that the amount of methine observed (in terms of its integral) increased as the temperature was raised. Heald *et al.*[36,37] conducted NMR studies and demonstrated changes in the nanoparticle conformation and structure with increasing temperature, and higher temperatures could increase the mobility of the PLA. Our NMR results

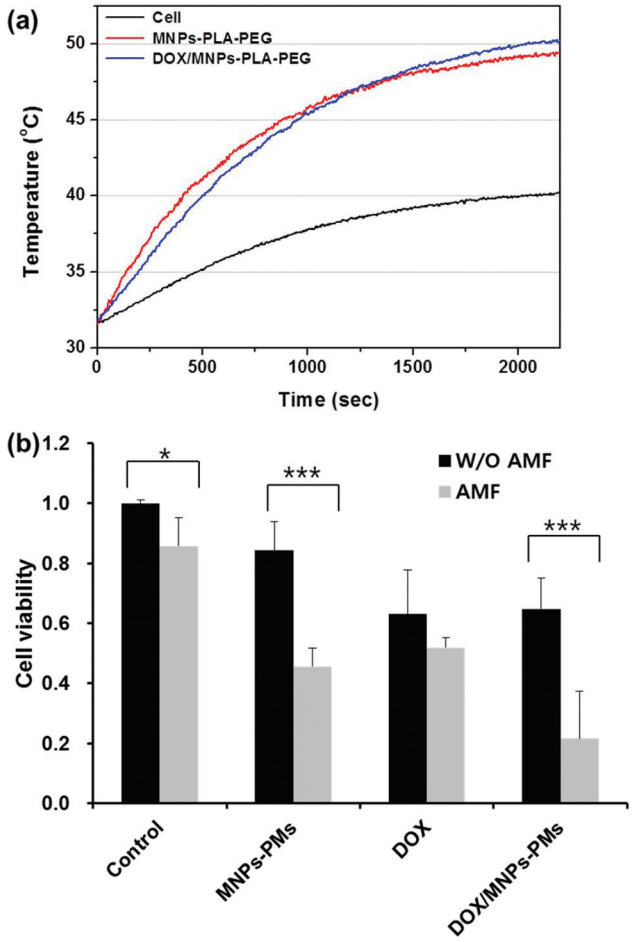

Fig. 7 Temperature profiles of cell culture media during the hyperthermia experiment (a) and cellular toxicity of free DOX, MNP-PLA-PEG, and DOX/MNP-PLA-PEG with or without exposure to AMF (b) (* and *** denotes $p < 0.05$ and $p < 0.001$, respectively; mean ± SD, $n = 3$).

reflect a change in the mobility of the PLA chain. Moreover, the change in chain mobility was confirmed by DSC measurement, which showed the appearance of an endothermic melting peak between 40 °C and 56 °C (Fig. S5 in the ESI†). Therefore, a change in the mobility of PLA at elevated temperature can have a critical influence on the stability of the incorporated drug molecules in the micellar core. The size and morphology of DOX/MNP-PMs were investigated before and after applying AMF by DLS and TEM (Fig. 4(c) and (b)). The size of DOX/MNP-PMs obtained *via* DLS and TEM measurement was about 93.5 nm and 80 nm, respectively, demonstrating that encapsulation of hydrophobic DOX increased the size relative to that of the MNP-PMs. After applying AMF, the average size of DOX/MNP-PMs increased to 391.7 nm, as determined by DLS. Furthermore, encapsulation of DOX to the MNPs resulted in a morphological change, as revealed in the TEM image (Fig. 4(d) inset), and larger aggregates were formed under AMF. These results indicate that DOX release is significantly enhanced due to the structural deformation related to the change in the mobility of PLA chains with increasing temperature in the presence of a magnetic field.

3.4 Cytotoxicity and cellular uptake

Prior to analyzing the hyperthermic effect of MNP-PMs, we examined the biocompatibility of the MNPs for human adenocarcinoma A549 cells. Cell viability was not significantly affected after A549 cells were incubated with MNP-PMs for 48 h at concentrations of 12.5, 25, 50 and 100 μg mL^{-1}, as measured by the MTS. Indeed, the viability was nearly 100% that of the control cell sample (Fig. 5(a)). This result indicates that MNP-PMs are not cytotoxic to A549 cells at concentrations as high as 100 μg mL^{-1}. To determine the extent of cellular uptake, the A549 cells were treated with fluorescence dye-encapsulated micelles for 2 h and observed under a confocal microscope. MNP-PMs were clearly observed inside the cells, but were not distributed in the nuclear compartment (Fig. 5(b). This result showed that MNP-PMs can penetrate the cellular membranes, but not the nuclear membrane. Furthermore, we investigated the cell viability with concentrations of free DOX and the DOX encapsulated in MNP-PMs (Fig. 6). A549 cell proliferation decreased to 18% of the control cell level with treatment of 0.8 μg mL^{-1} free DOX, but proliferation further decreased to 64% of the control cell level, when the same concentration of DOX was encapsulated in MNP-PMs. When the DOX concentration was increased to as high as 20 μg mL^{-1}, cell proliferation decreased to similar levels for free DOX and encapsulated DOX, at 7.5% and 7.8% of control levels, respectively.

3.5 *In vitro* hyperthermia under an AC magnetic field

An *in vitro* hyperthermia experiment was performed under an AC magnetic field in A549 cells with MNP-PMs and DOX/MNP-PMs. The A549 cells were treated with samples at a concentration of 25 μg mL^{-1} for 2 h at 37 °C and then exposed to an AMF at a frequency of 200 kHz and field strength of 1.5 kA m^{-1}. Fig. 7(a) shows the temperature profiles of MNP-PMs and DOX/MNP-PMs within the cancer cells under the AC magnetic field. The observed temperature variation for MNP-PMs and DOX/MNP-PMs was high enough to reach the desirable hyperthermia level within less than 600 s. In A549 cells, the temperature curve was below the hyperthermia level throughout the experiment. To measure the thermoablation after AMF application, the cells were re-plated on a 96-well culture plate in triplicate and incubated for a further 24 h. Cell viability compared to that of control cells measured by the MTS assay is shown in Fig. 7(b). The viability of the control cells subjected to the AMF decreased by 0.86-fold compared to the non-hyperthermic control cells ($p < 0.05$), whereas cells treated with MNP-PMs or DOX/MNP-PMs followed by AMF irradiation showed viabilities that were 0.46- and 0.22-fold lower than those of the non-hyperthermic cells, respectively ($p < 0.001$). However, cells treated with free DOX followed by AMF irradiation showed no significant change in viability compared to non-hyperthermic control cells. These results indicated that MNP-PMs induced significant hyperthermic effects to cause enhanced cytotoxicity. In addition, the DOX/MNP-PMs caused

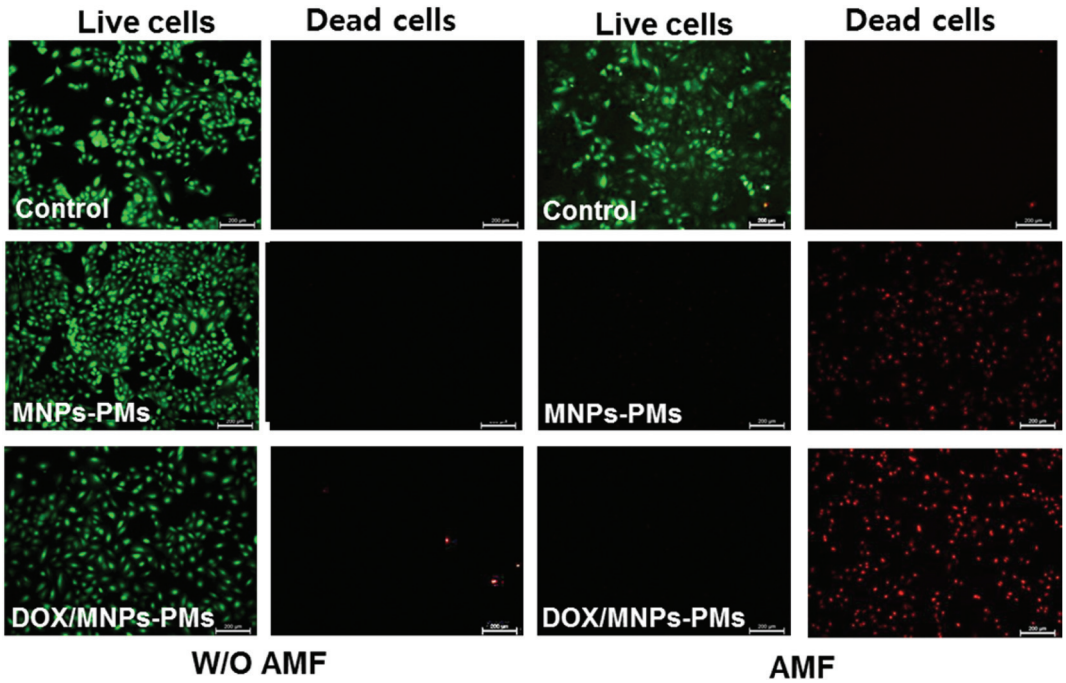

Fig. 8 Cell viability/death images after treating A549 cells with MNPs-PLA-PEG and DOX/MNP-PLA-PEG micelles with or without exposure to AMF (scale bar = 200 μm).

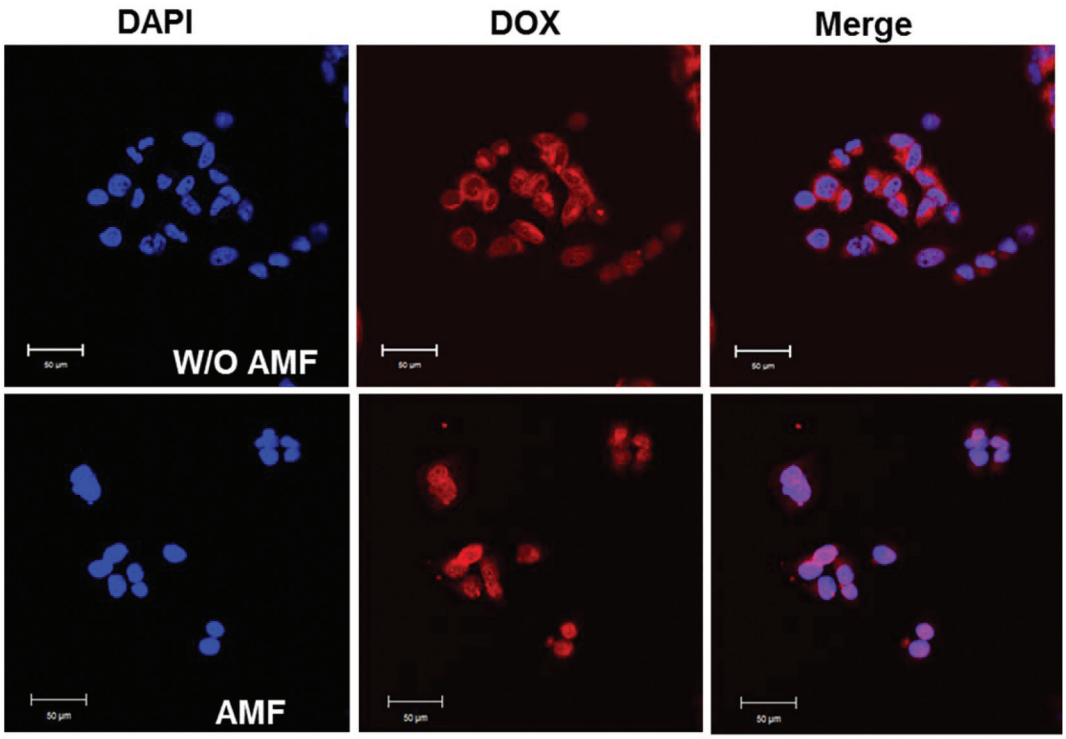

Fig. 9 Distribution of DOX/MNP-PLA-PEG micelles in A549 cells by confocal laser-scanning microscopy with or without exposure to AMF (scale bar = 50 μm).

a significant decrease in cell proliferation compared to free DOX *via* magnetic hyperthermia (from 0.52- to 0.22-fold; $p < 0.001$). These results show that DOX/MNP-PMs are more effective in the presence of AMF when compared to either the hyperthermia induced by MNP-PMs or chemotherapy with DOX/MNP-PMs alone. The cytotoxic effect exerted by AMF irradiation was observed by specific staining for live and dead cells (Fig. 8). The cells treated with only MNP-PMs showed an increased proportion of dead cells after AMF irradiation compared with control cells. Similar to the enhanced cytotoxic effect observed for DOX/MNP-PMs after AMF, the cells treated with DOX/MNP-PMs showed an increased proportion of dead cells compared to samples treated with only MNP-PMs after AMF exposure. This result indicates a synergistic effect from the combination of hyperthermia and chemotherapy. Fig. 9 shows the distribution of DOX in cells after AMF irradiation. DOX was observed mainly in the cytosol without AMF treatment, whereas most of the DOX signal was observed in the nuclear compartment after AMF irradiation. This result indicated that the encapsulation of DOX into MNP-PMs caused retardation of the penetration of free DOX into the nuclear membranes, whereas the release of DOX from DOX/MNP-PMs induced diffusion of the drug molecules by a heating effect from the AMF treatment, which facilitated the distribution of DOX in the nuclear compartment.

4. Conclusions

In the present study, we prepared MNP-conjugated PLA-PEG and investigated the drug release behavior of an incorporated anticancer drug (DOX) in MNP-PMs upon AMF. When AMF was applied to heat the DOX-loaded MNP-PMs at an intensity of 1.5 kA m^{-1} and a frequency of 200 kHz, the temperature was increased sufficiently to meet the conditions of hyperthermia. Indeed, drug release was enhanced under AMF, and the magnetically induced drug release resulted in rapid release of the drug molecules, accompanied by a change in the mobility of PLA chains by heating the MNPs under magnetic stimuli. *In vitro* cytotoxicity tests further indicated that DOX-loaded MNP-PMs induced enhanced apoptosis of cancer cells due to a synergistic effect of chemotherapy and hyperthermia, showing that the combined treatment strategy is more effective than either treatment alone.

Acknowledgements

This work was supported by the Ministry of Science, ICT, & Future Planning of the Republic of Korea (DGIST Basic Research Fund 14-NB-2 and 15-NB-2). The authors wish to thank Dr Jong Hun Lee for helpful discussions.

References

1 M. Arruebo, R. Fernández-Pacheco, M. R. Ibarra and J. Santamaría, *Nano Today*, 2007, **2**, 22.
2 J. Kim, J. E. Lee, S. H. Lee, J. H. Yu, J. H. Lee, T. G. Park and T. Hyeon, *Adv. Mater.*, 2008, **20**, 478.
3 S. Laurent, D. Forge, M. Port, A. Roch, C. Robic, L. van der Elst and R. N. Muller, *Chem. Rev.*, 2008, **108**, 2064.
4 J. Kim, Y. Piao and T. Hyeon, *Chem. Soc. Rev.*, 2009, **38**, 372.
5 R. Hergt, S. Dutz, R. Müller and M. Zeisberger, *J. Phys.: Condens. Matter*, 2006, **18**, S2919.
6 J. L. Roti Roti, *Int. J. Hyperthermia*, 2008, **24**, 3.
7 C. S. S. R. Kumar and F. Mohammad, *Adv. Drug Delivery Rev.*, 2011, **63**, 789.
8 E. Teodor, S.-C. Litescu, V. Lazar and R. Somoghi, *J. Mater. Sci. Mater. Med.*, 2009, **20**, 1307.
9 D. Qiu, X. An, Z. Chen and X. Ma, *Chem. Phys. Lipids*, 2012, **165**, 563.
10 E. Amstad, J. Kohlbrecher, E. Müller, T. Schweizer, M. Textor and E. Reimhult, *Nano Lett.*, 2011, **11**, 1664.
11 C. Huang, Z. Tang, Y. Zhou, X. Zhou, Y. Jin, D. Li, Y. Yang and S. Zhou, *Int. J. Pharm.*, 2012, **429**, 113.
12 Y. Zhou, Z. Tang, C. Shi, S. Shi, Z. Qian and S. Zhou, *J. Mater. Sci. Mater. Med.*, 2012, **23**, 2697.
13 C. Huang, Y. Zhou, Y. Jin, X. Zhou, Z. Tang, X. Guo and S. Zhou, *J. Mater. Chem.*, 2011, **21**, 5660.
14 F. Lu, A. Popa, S. Zhou, J.-J. Zhu and A. C. S. Samia, *Chem. Commun.*, 2013, **49**, 11436.
15 J. L. Arias, L. H. Reddy, M. Othman, B. Gillet, D. Desmaele, F. Zouhiri, F. Dosio, R. Gref and P. Couvreur, *ACS Nano*, 2011, **5**, 1513.
16 L. H. Reddy, J. L. Arias, J. Nicolas and P. Couvreur, *Chem. Rev.*, 2012, **112**, 5818.
17 P. Kulshrestha, M. Gogoi, D. Bahadur and R. Banerjee, *Colloids Surf., B*, 2012, **96**, 1.
18 K. Katagiri, Y. Imai, K. Koumoto, T. Kaiden, K. Kono and S. Aoshima, *Small*, 2011, **7**, 1683.
19 Y.-J. Kim, M. Ebara and T. Aoyagi, *Adv. Funct. Mater.*, 2013, **23**, 5753.
20 T.-Y. Liu, K.-H. Liu, D.-M. Liu, S.-Y. Chen and I.-W. Chen, *Adv. Funct. Mater.*, 2009, **19**, 616.
21 H. Oliveira, E. Pérez-Andrés, J. Thevenot, O. Sandre, E. Berra and S. Lecommandoux, *J. Controlled Release*, 2013, **169**, 165.
22 A. Baeza, E. Guisasola, E. Ruiz-Hernández and M. Vallet-Regí, *Chem. Mater.*, 2012, **24**, 517.
23 S. D. Kong, W. Zhang, J. H. Lee, K. Brammer, R. Lal, M. Karin and S. Jin, *Nano Lett.*, 2010, **10**, 5088.
24 C. R. Thomas, D. P. Ferris, J.-H. Lee, E. Choi, M. H. Cho, E. S. Kim, J. F. Stoddart, J.-S. Shin, J. Cheon and J. I. Zink, *J. Am. Chem. Soc.*, 2010, **132**, 10623.
25 Y. Yamamoto, K. Yasugi, A. Harada, Y. Nagasaki and K. Kataoka, *J. Controlled Release*, 2002, **82**, 359.
26 M. Yokoyama, T. Okaiio, Y. Sakurai, H. Ekimoto, C. Shibazaki and K. Kataoka, *Cancer Res.*, 1991, **51**, 3229.
27 K. Kataoka, G. S. Kwon, M. Yokoyama, T. Okano and Y. Sakurai, *J. Controlled Release*, 1993, **24**, 119.
28 G. S. Kwon, S. Suwa, M. Yokoyama, T. Okano, Y. Sakurai and K. Kataoka, *J. Controlled Release*, 1994, **29**, 17.

29 X. Zhang, J. K. Jackson and H. M. Burt, *Int. J. Pharm.*, 1996, **132**, 195.
30 J. Park, K. An, Y. Hwang, J.-G. Park, H.-J. Noh, J.-Y. Kim, J.-H. Park, N.-M. Hwang and T. Hyeon, *Nat. Mater.*, 2004, **3**, 891.
31 M. Lattuada and T. A. Hatton, *Langmuir*, 2007, **23**, 2158.
32 D. Singh, R. K. Gautam, R. Kumar, B. K. Shukla, V. Shankar and V. Krishna, *J. Water Proc. Eng.*, 2014, **4**, 233.
33 A. Prokop and J. M. Davidson, *J. Pharm. Sci.*, 2008, **97**, 3518.
34 S. Bae, S. W. Lee, A. Hirukawa, Y. Takemura, Y. H. Jo and S. G. Lee, *IEEE T. Nanotechnol.*, 2009, **8**, 86.
35 S. Purushotham and R. V. Ramanujan, *J. Appl. Phys.*, 2010, **107**, 114701.
36 T. Riley, S. Stolnik, C. R. Heald, C. D. Xiong, M. C. Garnett, L. Illum and S. S. Davis, *Langmuir*, 2001, **17**, 3168.
37 C. R. Heald, S. Stolnik, K. S. Kujawinski, C. De Matteis, M. C. Garnett, L. Illum, S. S. Davis, S. C. Purkiss, R. J. Barlow and P. R. Gellert, *Langmuir*, 2002, **18**, 3669.